*This paper was presented at the Second International Symposium on Risk Analysis and Safety of Complex Structures and Components (IRAS 2023), 2-4 April 2023, Belgrade, Serbia*

*Aleksandar Maslarević[1*], Gordana Bakić[2], Bratislav Rajičić[1], Nenad Milošević[2], Vesna Maksimović[3]*

# INFLUENCE OF PLASMA TRANSFERRED ARC WELDING PARAMETERS ON THE OBTAINED MICROSTRUCTURE OF 316L COATING

# UTICAJ PARAMETARA ZAVARIVANJA PLAZMOM NA MIKROSTRUKTURU OBLOGE OD ČELIKA 316L

Originalni naučni rad / Original scientific paper
UDK /UDC:

Rad primljen / Paper received: 22.05.2023

Adresa autora / Author's address:
[1)] University of Belgrade, Innovation Centre of the Faculty of Mechanical Engineering, Belgrade, Serbia
[*]email: amaslarevic@mas.bg.ac.rs
[2)] University of Belgrade, Faculty of Mechanical Engineering, Belgrade, Serbia
[3)] Vinča Institute of Nuclear Sciences, Belgrade, Serbia

**Keywords**
- plasma transferred arc (PTA)
- microstructure
- coating hardness
- steel 316L
- welding current

**Ključne reči**
- plazma luk
- mikrostruktura
- tvrdoća prevlake
- čelik 316L
- jačina struje zavarivanja

*Abstract*

*The paper describes the surfacing technology for coating of high-alloyed austenitic stainless steel 316L on the steel S235JR base material. Coatings were applied by plasma transferred arc welding process. The 5 samples were made using different welding currents while other welding parameters were constant. Metallographic analysis of the obtained samples is used to establish a correlation between the microstructural constituents and the applied welding current in the surfacing process. According to this it was possible to determine the optimal parameters of coating surfacing. The filler material was in the form of powder, while its characterization was performed by scanning electron microscopy, and the characterization of the obtained coatings by optical microscopy.*

*Izvod*

*Ovaj rad opisuje tehnologiju navarivanja prevlake od visokolegiranog austenitnog nerđajućeg čelika 316L na osnovni materijal od čelika S235JR. Prevlaka je nanesena tehnikom navarivanja plazmom. Izrađeno je 5 epruveta sa različitim vrednostima jačine struje, dok su ostali parametri navarivanja bili konstantni. Metalografska analiza dobijenih epruveta je iskorišćena za uspostavljanje korelacije između mikrostrukture i jačine struje tokom procesa navarivanja. Na osnovu toga je bilo moguće odrediti optimalne parametre za navarivanje. Korišćen je dodati materijal u obliku praha i njegova karakterizacija je izvršena uz pomoć skenirajućeg elektronskog mikroskopa, dok je karakterizacija samog navarenog sloja urađena primenom optičkog mikroskopa.*

## INTRODUCTION

An aggressive corrosive environment often causes reduced service life of many machine parts and assemblies. One of the possible ways to extend the service life is to apply protective coatings to material surfaces that work in a corrosive environment. Protective coatings can be applied either during the manufacturing process itself, or during the repair of parts. One example of how protective coatings can be applied in the manufacture of a machine part that needs to work in an aggressive corrosion environment, is to make the part from cheap carbon steel with weak corrosion resistance, and to apply a coating that has increased corrosion resistance to surfaces which will be exposed to corrosion (e.g. high-alloy stainless steel), /1-3/.

Protective coatings can be applied by different methods, often welding and thermal spraying. To date, a large number of welding methods have been developed that are also used to apply coatings. From the quality point of view, tungsten inert gas welding (TIG) stands out from conventional methods, and plasma transferred arc (PTA) from special methods, /4-9/. Due to a number of advantages, PTA has found a very wide application in the field of applying protective coatings /10/, and also in the surfacing of intermediate layers (buffer layers). The PTA is a modified version of plasma welding and has been in use for over 60 years. The development of this method was prompted by the need to apply protective layers to components in nuclear facilities /11/. Compared to conventional welding methods, PTA can achieve lower heat input, greater deposition, lower depth of penetration, and a lower dilution, /12-14/. Also, if we compare PTA with thermal spraying methods, it can be concluded that PTA is characterised by higher productivity and lower cost /15, 16/. In general, due to the wide range of additional materials and their low price, as well as due to the extremely high-quality coatings, PTA has an increasing application in the protection of surfaces from corrosion or wear, /17/.

Steel 316L (ASTM/ASME), which belongs to the group of austenitic stainless steels, is intensively used in a variety of industry fields, like the nuclear /18/, chemical and petrochemical /19-20/, pharmaceutical /21/, and also in the pro-

duction of medical implants /22/, and in the production of components for thermal power plants, /23/, etc.

This paper describes the technology of surfacing by coating 316L with PTA, with varying the welding current, while other surfacing parameters remain unchanged. In addition to the description of the surfacing technology, a microstructural characterization of the applied coatings was performed, where changes in microstructure were observed depending on the applied welding current in the surfacing process. Also, the dependence of changes in coating hardness with welding current in different zones of the sample, in the direction of the base material (BM), heat affected zone (HAZ), coating, was analysed.

## MATERIALS AND METHODS

In the process of surfacing the coating, a plate made of S235JR steel (SRPS EN 10025-2) of size 50×100 mm and thickness of 10 mm, was used as BM, while FeCrNiMo powder was used as filler material (FM), which corresponds to stainless steel 316L (ASTM/ASME standards). The filler material is produced by Castolin Eutectic Co. with the trademark EuTroLoy 16316 and is intended for surfacing steels used in the food and chemical industries. According to the manufacturer Castolin Eutectic, the nominal size range of FM particles is 32-125 μm, /24/. The chemical composition of BM and FM is shown in Table 1.

The coatings were applied by the PTA, using the device EuTronic Gap 3001 DC manufactured by Castolin Eutectic, Fig. 1. The device is connected to the unit for numerical control of the torch movement, which controls the movement in three directions during the surfacing.

The preparation of the BM for surfacing consisted of grinding the surface with the aim of removing surface impurities and oxides. Also, in order to avoid deformation of the samples during the surfacing process, all samples were welded to a 150×500×6 mm plate.

Table 1. Chemical composition of the BM and FM, /24, 25/.

| Base material | Chemical element (%) | | | | | |
|---|---|---|---|---|---|---|
| | $C_{max}$ | Mn | $P_{max}$ | $S_{max}$ | Cu | Fe |
| S235JR | 0.17 | 1.40 | 0.035 | 0.035 | 0.55 | residue |
| Filler material | Chemical element (%) | | | | | |
| | C | Cr | Ni | Mo | Fe | |
| 316L | 0.03 | 17.5 | 13.0 | 2.7 | residue | |

Figure 1. PTA welding device with numerical control unit, /3, 23/.

In the surfacing process, the welding current was varied in the range from 80 to 120 A, while all other parameters remained unchanged, and the 316L coating was applied to five samples, (I-V, Table 2). On all samples, a middle surface was over plated 80×28 mm, and surfacing was carried out continuously without interruption.

Table 2. PTA surfacing parameters.

| PTA surfacing parameters | Sample number | | | | |
|---|---|---|---|---|---|
| | I | II | III | IV | V |
| Welding current (A) | 80 | 90 | 100 | 110 | 120 |
| Arc voltage (V) | 27.5 | | | | |
| Powder feeding rate (g/min) | 35 | | | | |
| Plasma gas | Ar | | | | |
| Plasma gas flow rate (l/min) | 2 | | | | |
| Shield and carrier gas | 95 % Ar + 5 % $H_2$ | | | | |
| Shield gas flow rate (l/min) | 15 | | | | |
| Carrier gas flow rate (l/min) | 2.5 | | | | |
| Speed of torch movement in the sample length direction (mm/s) | 0.6 | | | | |
| Speed of torch movement in the sample width direction (mm/s) | 15 | | | | |
| Width of the welding zone (mm) | 28 | | | | |
| Number of passes | 1 | | | | |

Before the coating, the FM was characterized using a scanning electron microscope (SEM) type SEM JEOL JSM 5800LV. Metallographic testing by optical microscopy was performed with a Metaval Carl Zeiss Jena light microscope. The samples were prepared by wet grinding, polishing, and etching. For wet sanding, SIC sandpaper with a fineness of 80 to 1000 was used on the Phoenix 4000 device, manufactured by Buehler. The final polishing was done with alumina ($Al_2O_3$) granulation 1 μm in water suspension. A solution of picric acid in ethyl alcohol (picric acid 4 % HCl + ethanol) was used as an etching agent for coatings, while nital (a 3 % solution of nitric acid $HNO_3$ in ethyl alcohol) was used for etching of the BM.

Hardness measurements in the cross-section of samples was performed using the Vickers method, on a TP-7R-1 device manufactured by Tochpribor with a load of 9.807 N for 10 s. The hardness was measured at 5 characteristic areas in the sample cross-section, Fig. 2: 1-BM, 2-HAZ, 3-coating layer, immediately above the fusion line, 4-the middle of the coating thickness, and 5-coating layer near the coating surface. Three measurements were performed for each area.

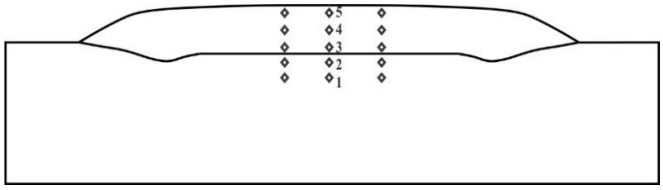


Figure 2. Hardness measurements - arrangement of measuring points, /3/.

## RESULTS AND DISCUSSION

Figure 3 shows the particles of the powder used as FM at different magnifications. Most of the powder particles are spherical, as a consequence of obtaining the powder by the

atomization process, /24/. The spheres are mostly regular in shape, have a compact dendritic structure, and porosity is observed on their surface.

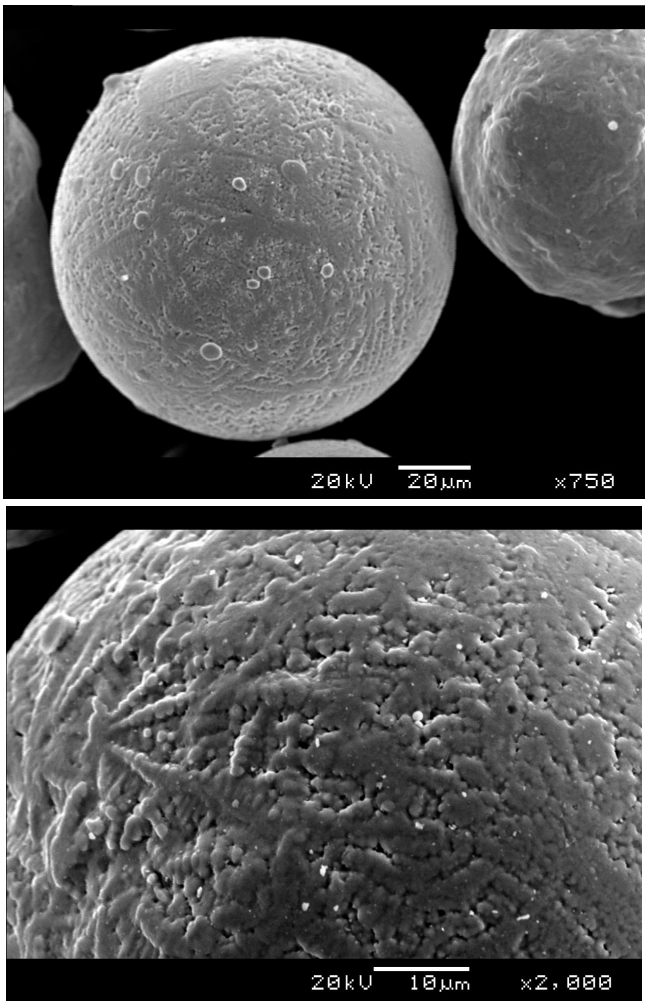


Figure 3. SEM of powder particles of the 316L FM.

Microstructural tests of the 316L coating included tests of all weld zones, base metal, and HAZ. The base metal has a ferrite-pearlite structure, while a coarse-grained HAZ structure can be observed near the fusion line, as shown in Fig. 4 for the sample obtained by welding current 100 A. One can see that the width of the HAZ grows with an increase in heat input, as a consequence of increased welding current.

Figures 5-9 show the microstructure of the 316L coating in different zones for all five samples. The microstructure of the samples consists of austenite grains of fine cellular structure, as a consequence of the cooling rate during the solidification of the weld metal. At rapid cooling there are conditions for the development of non-equilibrium phases, i.e. the intercellular separation of Mo, Cr, and Si, and the creation of eutectic ferrite (δ ferrite), /26, 27/. In all five cases, the applied coatings are compact in the absence of porosity and inclusions.

Along the fusion zone, polygonal austenite structure can be observed in all coatings, growing into a dendritic cell moving away from the BM, with a change in dendrite size for different welding currents, Figs. 5-9, /3, 28, 29/. At higher welding currents, the cell structure of uneven size is more pronounced with the presence of grains growing in the direction of the heat removal. The oriented grain growth can be observed in zones near the top of the coating, Figs. 5-9.

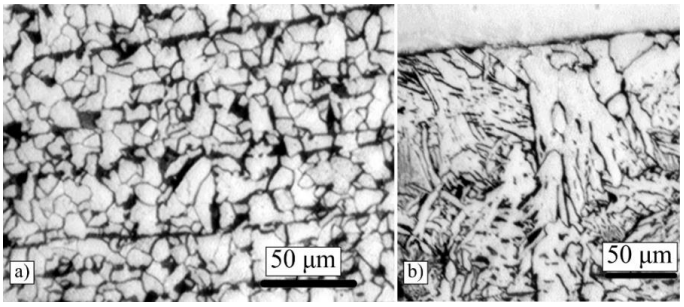


Figure 4. Microstructure at 100 A current: a) BM; b) HAZ.

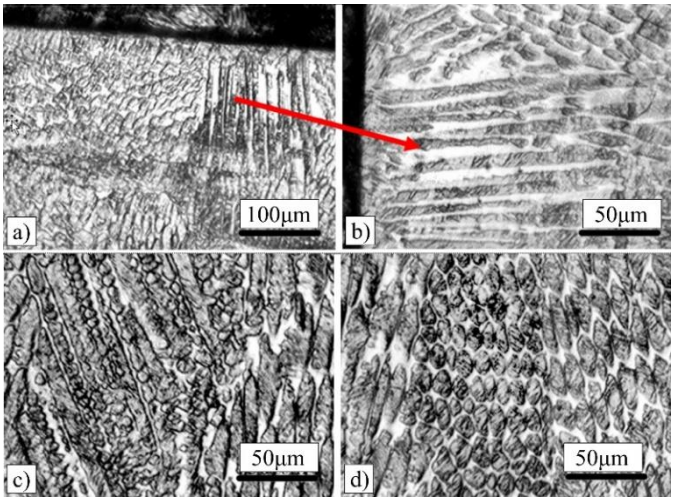


Figure 5. Coating microstructure, welding current 80 A.

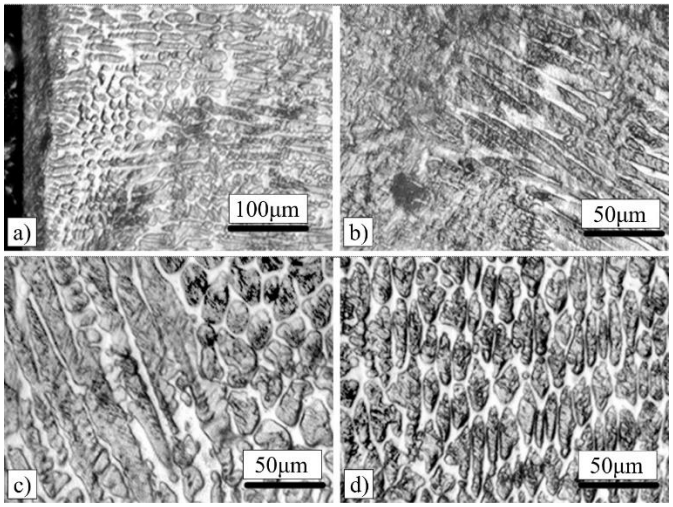


Figure 6. Coating microstructure, welding current 90 A.

Using the Scheffler diagram for this alloy, it is possible to determine the expected proportion of δ-ferrite. The ratio of Cr and Ni equivalents content in the steel composition ($Cr_{eq}/Ni_{eq}$) determines the amount of δ-ferrite in the weld metal, and in this case it is about 1.42. In the case of 316L steel, if the $Cr_{eq}/Ni_{eq}$ ratio is < 1.3, it is possible to expect a purely austenitic structure, /26/. In our case, this ratio is 1.42 which indicates that an austenite-ferrite structure was

formed by solidification according to the following sequence L → L+δ → L+δ+γ → γ+δ, /26/. At lower cooling rates, δ-ferrite transforms into austenite, in contrast to the higher cooling rates when δ-ferrite remains present in the formed microstructure, such as the case of crystallization and cooling

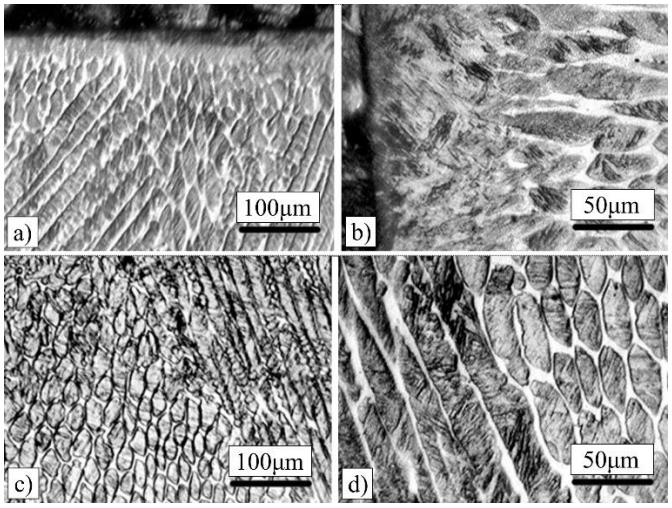


Figure 7. Coating microstructure, welding current 100 A.

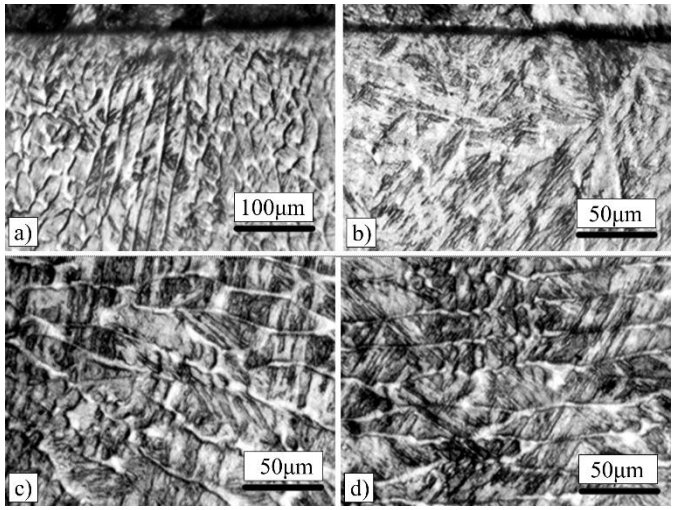


Figure 8. Coating microstructure, welding current 110 A.

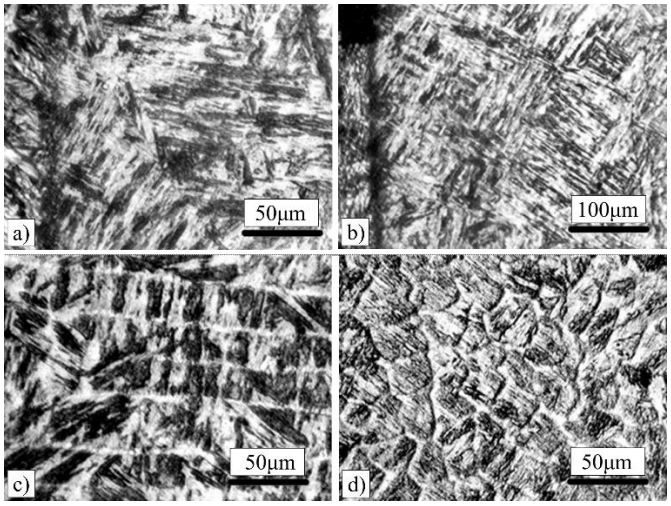


Figure 9. Coating microstructure, welding current 120 A.

of coatings obtained by welding with higher currents, which corresponds to the experimental conditions in this work. In the fusion zone, due to the mixing of BM and FM, the content of Cr and Ni in the alloy locally decreases and the content of C increases. As the content of Cr and Ni in the alloy decreases, the possibility of appearing ferrite increases. Increase in the amount of C stabilizes austenite to a greater extent, so a negligible amount of δ-ferrite is expected in the fusion zone regardless of the cooling rate. In zones above the fusion zone, where carbon content is lower, according to Scheffler's diagram, conditions for martensite formation are fulfilled, as can be seen partially in Figs. 8 and 9.

In the zone below the top of the coating, cell width was determined, whereby an approximately linear dependence of the welding current and cell width was observed, Fig. 10. With an increase in welding current, a coarser dendritic microstructure of the coating is formed due to increased heat input, but also due to the lower thermal conductivity of the 316L alloy. The quantity of heat input directly affects the formed intercellular distance. Given that, due to lower mechanical properties, it is desirable to avoid a coarse-grained and martensitic microstructure in the coating, it can be stated that the optimal currents for applying this coating by PTA welding are I ≤ 100 A.

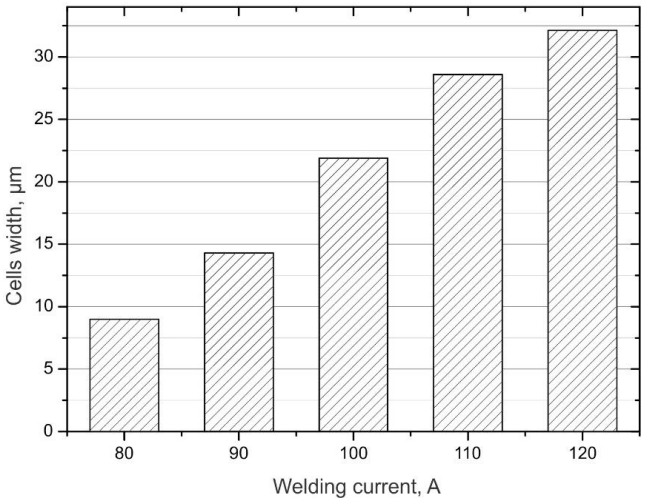


Figure 10. Cell width dependence with welding current.

Figure 11 shows the change in average hardness values across the sample cross section. According to the manufacturer's declaration, the hardness of this alloy should be around 170 HV. However, significant higher values were achieved primarily due to dilution, but also due to possible separation of Mo, Cr, and Si in the interdendritic region, as well as the appearance of martensite, due to higher cooling rates.

Despite the application of different welding currents in the surfacing process, the different heat input, the hardness of BM at point 1, and HAZ at point 2, is practically the same for all five samples. Although higher hardness values are expected in the HAZ zone obtained with a higher heat input, it was not observed in this case.

The highest hardness was measured in all samples (except for the sample where the welding current was 100 A), a little above the fusion line (at point 3, Fig. 11), because the high-

est dilution of BM and FM was achieved in this zone. A large increase in hardness was observed in all areas of the coating for welding currents of 100 A and above. The present differences in measured hardness values are the result of different heat inputs (insufficient, optimal, and excessive), different speeds of diffusion processes, as well as due to different cooling rates which irreversibly reflects on the microstructure of the coating and residual stresses. All of this indicates that for welding currents of 100 A and above it is not possible to achieve a coating quality that corresponds to the composition and properties of steel 316L in one layer. In the cell size determination zone, the coating hardness was also measured (point 5, Fig. 11b). Dependence of coating hardness (point 5) on the width of the cells achieved at different welding currents is shown in Fig. 12. With the increase in welding current, due to increased heat input, a coarser dendritic structure is formed, which significantly changes the properties and hardness of the coating. The dilution effect and the heat input directly affect the formed intercellular distance.

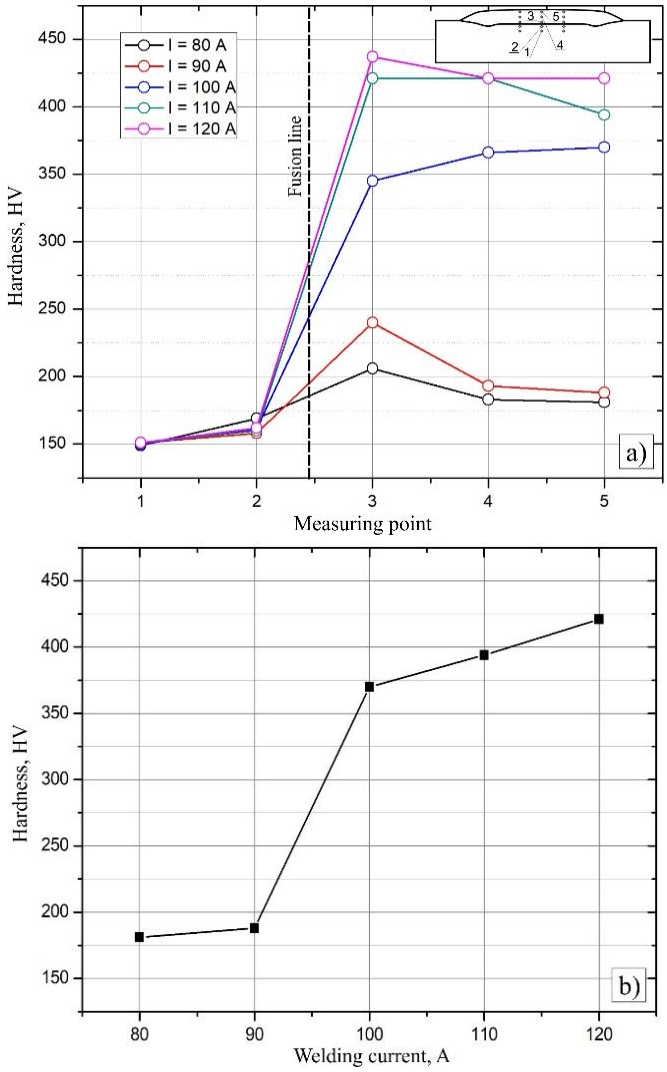


Figure 11. Coating hardness values: a) measured at five points; b) at the top of the coating (point 5).

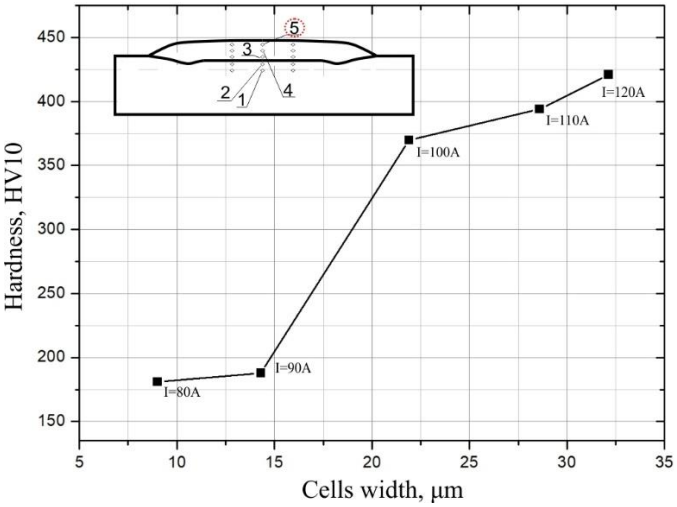


Figure 12. Dependence of coating hardness at measuring point 5 on the cell width.

It is possible to indirectly, semi-quantitatively, determine the microstructure achieved for a certain welding current by measuring the hardness of coating surface layers. This data enables the correction of welding parameters with the aim of achieving the desired properties of the coating, but also a constant, simple check of the coating properties by measuring the hardness on-site.

## CONCLUSIONS

Based on the experimental results obtained by 5 testing samples surfaced by PTA, where the stainless steel 316L was used as FM, and steel S235JR as BM, the following can be concluded:

- it is possible to apply coatings of austenitic stainless steel 316L on carbon steel S235JR by PTA surfacing, without porosity, inclusions, and similar defects, which ensures better corrosion resistance of the surface;
- a cellular dendritic structure of the coating is obtained for all five welding currents, from 80 to 120 A, with an approximately linear dependence of the current and cell size;
- the presence of a martensitic microstructure in the coating is observed at higher welding currents (110-120 A), which should be avoided, and for that reason welding currents $I \leq 100$ A are recommended. However, this value should be the lowest in order to avoid higher hardness;
- correlation between microstructural parameters (cell width) and hardness of the coating 316L was established which enables a simple evaluation of coating properties by measuring the hardness on-site.

## ACKNOWLEDGEMENTS

This work was the result of research supported by the Ministry of Science, Technological Development and Innovation of the Republic of Serbia under Contract No.451-03-47/2023-01/200105, dated February 3, 2023.

## REFERENCES

1. McIlwain, J.F., Neumeier, L.A., Plasma-sprayed iron-base wear-resistant coatings containing titanium diboride, US Bureau of Mines, Report of Investigations, 8984, 1985.

2. Maslarević, A., Bakić, G., Djukić, M., et al. (2018), *Characterization of a coating 316l applied by plasma transferred arc*, Hemijska industrija, 72(3): 139-147. doi: 10.2298/HEMIND170928005M (in Serbian)
3. Maslarević, A., Bakić, G., Sijački Žeravčić, V., et al. (2015), *Plasma transferred arc hardfacing with 316L*, In: Proc. 3rd IIW South-East Europ. Welding Congress, 'Welding and Joining Technologies for a Sustainable Development and Environment', ISIM, Timisoara, Romania, 2015, pp. 283-288. doi: 10.13140/RG.2.1.3808.1520
4. Pawlowski, L., The Science and Engineering of Thermal Spray Coatings, 2nd Ed., John Wiley & Sons Ltd., London, 2008. doi: 10.1002/9780470754085
5. Fauchais, P.L., Heberlein, J.V.R., Boulos, M.I., Thermal Spray Fundamentals - From Powder to Part, Springer, New York, NY, 2014. doi: 10.1007/978-0-387-68991-3
6. Bakić, G., Maksimović, V., Maslarević, A., et al. (2015), *Microstructural characterization of WC and CrC based coatings applied by different processes*, In: Proc. and Book of Abstract of Metallurgical and Materials Eng. Congress of South-East Europe, MME SEE 2015, Belgrade, Serbia, pp.195-201.
7. Maslarević, A., Bakić, G., Lukić, U., Martić, I. (2014), *Impact of parameters of plasma transferred arc welding process on the weld layer geometry*, In: Proc. 18th Int. Research/Expert Conf., 'Trends in the Development of Machinery and Associated Technology', TMT 2014, Budapest, Hungary, pp. 445-448.
8. Ulutan, M., Kiliçay, K., Çelik, O.N., Er, Ü. (2016), *Microstructure and wear behaviour of plasma transferred arc (PTA)-deposited FeCrC composite coatings on AISI 5115 steel*, J Mater. Process. Technol. 236: 26-34. doi: 10.1016/j.jmatprotec.2016.04.032
9. Maslarević, A., Bakić, G., Djukić, M., et al. (2020), *Microstructure and wear behavior of MMC coatings deposited by plasma transferred arc welding and thermal flame spraying processes*, Trans. Indian Inst. Met. 73: 259-271. doi: 10.1007/s12666-019-01831-9
10. Balasubramanian, V., Lakshminarayanan, A.K., Varahamoorthy, R., Babu, S. (2009), *Application of response surface methodolody to prediction of dilution in plasma transferred arc hardfacing of stainless steel on carbon steel*, J Iron Steel Res., Int. 16(1): 44-53. doi: 10.1016/S1006-706X(09)60009-1
11. Harris, P., Smith, B.L. (1983), *Factorial techniques for weld quality prediction*, Metal Constr. 15(11): 661-666.
12. D'Oliveira, A.S.C.M., Paredes, R.S.C., Santos, R.L.C. (2006), *Pulsed current plasma transferred arc hardfacing*, J Mater. Process. Tech. 171(2): 167-174. doi: 10.1016/j.jmatprotec.2005.02.269
13. Sudha, C., Shankar, P., Rao, R.V.S., et al. (2008), *Microchemical and microstructural studies in a PTA weld overlay of Ni-Cr-Si-B alloy on AISI 304L stainless steel*, Surf. Coat. Tech. 202(10): 2103-2112. doi: 10.1016/j.surfcoat.2007.08.063
14. Hállen, H., Lugscheider, E., Ait-Mekideche, A. (1991), *Plasma transferred arc surfacing with high deposition rates*, In: T. Bernecki (Ed.), Proc. Fourth National Thermal Spray Conf., Pittsburgh, PA, ASM Int., Materials Park, OH, USA, 1991, pp. 427-434.
15. Veinthal, R., Sergejev, F., Zikin, A., et al. (2013), *Abrasive impact wear and surface fatigue wear behaviour of Fe-Cr-C PTA overlays*, Wear, 301(1-2): 102-108. doi: 10.1016/j.wear.2013.01.077
16. Maslarević, A., Rajičić, B., Bakić, G., et al. (2015), *High velocity oxygen fuel (HVOF) spraying*, Int. Scientific Conf. of IT and Business-Related Research - Synthesis 2015, Belgrade, Serbia, 2015, pp.262-267. doi: 10.15308/Synthesis-2015-262-267
17. Badisch, E., Ilo, S., Polak, R. (2009), *Multivariable modeling of impact-abrasion wear rates in metal matrix-carbide composite materials*, Tribol. Lett. 36: 55-62. doi: 10.1007/s11249-009-9458-y
18. Xu, J., Zhuo, C., Tao, J., et al. (2009), *Improving the corrosion wear resistance of AISI 316L stainless steel by particulate reinforced Ni matrix composite alloying layer*, J Phys. D: Appl. Phys. 42(1): 015410. doi: 10.1088/0022-3727/42/1/015410
19. Abosrra, L., Ashour, A.F., Mitchell, S.C., Youseffi, M. (2009), *Corrosion of mild steel and 316L austenitic stainless steel with different surface roughness in sodium chloride saline solutions*, WIT Trans. Eng. Sci. 65: 161-172. doi: 10.2495/ECOR090161
20. Xu, C., Zhang, Y., Cheng, G., Zhu, W. (2006), *Corrosion and electrochemical behavior of 316L stainless steel in sulfate-reducing and iron-oxidizing bacteria solutions*, Chinese J Chem. Eng. 14(6): 829-834. doi: 10.1016/S1004-9541(07)60021-4
21. Mathiesen, T., Rau, J., Frantsen, J.E., et al. (2002), *Using exposure tests to examine rouging of stainless steel*, Pharm. Eng. 21(4): 1-6.
22. Kurgan, N., Sun, Y., Cicek, B., Ahlatci, H. (2012), *Production of 316L stainless steel implant materials by powder metallurgy and investigation of their wear properties*, Chinese Sci. Bull. 57: 1873-1878. doi: 10.1007/s11434-012-5022-5
23. Maslarević, A., Modern deposition technologies for coatings and their potential application in thermal power plants, PhD Thesis, University of Belgrade, Faculty of Mechanical Eng., 2018. (in Serbian)
24. Datasheet Metal Powder, EuTroLoy 16316, Castolin Eutectic, GmbH, Vienna, 2005.
25. SRPS EN 10025-2:2020, Hot rolled products of structural steels - Part 2: Technical delivery conditions for non-alloy structural steels.
26. Kurzynowski, T., Gruber, K., Stopyra, W., et al. (2018), *Correlation between process parameters, microstructure and properties of 316 L stainless steel processed by selective laser melting*, Mater. Sci. Eng. A, 718: 64-73. doi: 10.1016/j.msea.2018.01.103
27. Miller, I.H. (2015), *The many facets and complexities of 316L and the effect on properties*, In: Proc. Int. Thermal Spray Conf. ITSC2015, CA, USA, 2015, ASM Int., pp.725-731. doi: 10.31399/asm.cp.itsc2015p0725
28. Pinkerton, A.J., Li, L. (2003), *The effect of laser pulse width on multiple-layer 316L steel clad microstructure and surface finish*, Appl. Surf. Sci. 208-209: 411-416. doi: 10.1016/S0169-4332(02)01422-8
29. Kell, J., Tyrer, J.R., Higginson, R.L., Thomson, R.C. (2005), *Microstructural characterization of autogenous laser welds on 316L stainless steel using EBSD and EDS*, J Microsc. 217(2): 167-173. doi: 10.1111/j.1365-2818.2005.01447.x